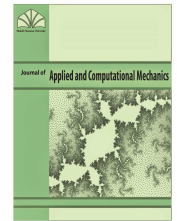




# Journal of Applied and Computational Mechanics



Research Paper

## An Experimental Comparison between Wing Root and Wingtip Corrugation Patterns of Dragonfly Wing at Ultra-low Reynolds Number and High Angles of Attack

Mohammad Hojaji<sup>1,2</sup>, Mohammad Reza Soufivand<sup>3</sup>, Roham Lavimi<sup>4</sup>

<sup>1</sup> Department of Mechanical Engineering, Najafabad Branch, Islamic Azad University, Najafabad, Iran, Email: hojaji\_m@pmc.iaun.ac.ir

<sup>2</sup> Aerospace and Energy Conversion Research Center, Najafabad Branch, Islamic Azad University, Najafabad, Iran

<sup>3</sup> Department of Mechanical Engineering, Najafabad Branch, Islamic Azad University, Najafabad, Iran, Email: m.r.soufivand@smc.iaun.ac.ir

<sup>4</sup> Département de Génie Mécanique, Université de Sherbrooke, Sherbrooke, J1K 2R1, Canada, Email: roham.lavimi@usherbrooke.ca

Received June 11 2020; Revised October 11 2020; Accepted for publication October 11 2020.

Corresponding author: M. Hojaji (hojaji\_m@pmc.iaun.ac.ir)

© 2021 Published by Shahid Chamran University of Ahvaz

**Abstract.** This study presents the empirical comparison between the wing root and wingtip corrugation patterns of dragonfly wing in the newly-built wind-tunnel at the IAUN. The main objective of the research is to investigate the effect of wingtip and wing root corrugations on aerodynamic forces and the flow physics around the cross-sections at  $Re=10000$  and the angle of attack of  $0^\circ$  to  $30^\circ$ . For this aim, two cross-sections are extracted from wing root (first cross-section) and wingtip (second cross-section). The first cross-section has corrugations with higher density than the second cross-section. The comparison of lift coefficients obtained from pressure distribution and force measurement indicates an acceptable agreement between the results. Also, Particle Image Velocity (PIV) technique is used to measure the velocity field. The results show that all corrugation patterns do not have positive effects on the aerodynamic forces. The second cross-section can generate considerable aerodynamic forces compared to the first cross-section. At  $\alpha=25^\circ$ , the lift coefficient generated by the second cross-section is 90% and 25% higher than that of the first cross-section and the flat plate, respectively. Based on results, corrugations in the wing root's vicinity have a crucial role in the solidity of insect wings; however, corrugations in the wing tip's vicinity play a vital role in generating adequate aerodynamic forces. The comparison conducted in the current research reveals the second cross-section is an appropriate replacement for the flat plate in MAVs due to generating more essential forces for flight.

**Keywords:** Dragonfly wings, Corrugations, MAVs, Flow physics, PIV, Ultra-low Reynolds.

### 1. Introduction

The use of Micro Air Vehicles (MAVs) has increasingly grown during the last decades. These types of aerial vehicles have broad applications such as data collection in environmental monitoring. The size of MAVs is significantly reducing so that their length does not currently exceed 6 inches. It should be noticed that they fly in Reynolds, in which the transition or turbulent flows may occur [1]. One of the prominent parts of MAVs is their wings; therefore, various wings have been designed and fabricated. However, almost all of them have poor aerodynamic performance and maneuverability limitations [2, 3].

Birds and insects are successful flyers that can show amazing flight stability and maneuverability [4]. Therefore, Insects flight has received considerable attention from researchers [5-9]. One of the most maneuverable flyers are dragonflies that can perform forward, backward, and hovering flights [10, 11]. Also, dragonflies and several other insects, such as locusts and damselflies, have unique wings. Their wings have a variety of corrugations along span-wise and chord-wise directions. These corrugations play a crucial role in the stability of ultra-light wings and significantly increase their stiffness and strength. Besides, they also handle bending forces during the flight [12, 13]. These geometry characteristics have given rise to a great deal of interest among researchers to investigate their properties [14]. Obtaining accurate information on how dragonflies fly results in the design and fabrication of wings that can generate adequate essential aerodynamic forces for MAVs. Hence, to fully comprehend characteristics of dragonfly wings, the flow physics around dragonfly wings should be experimentally and numerically investigated [15].

A myriad of studies with contradictory results has been empirically and numerically done on corrugated wings under different motions in recent years. A few studies have argued that corrugated wings have poor aerodynamic performance in a gliding motion, so they are not appropriate for MAVs [16-18]. However, several other studies have provided quite contradictory results, indicating that the wings with corrugations have better aerodynamic performance than conventional wings at lower Reynolds numbers [19, 20]. Buckholz [21] has experimentally studied corrugated wings at  $Re = 1500$ . The results showed that



corrugations enhance the lift coefficient. In another experimental study, Ekamoto and Azuma [22] have also reached the same results. They showed that corrugations significantly enhance the aerodynamic characteristics of the flat plate.

Consistent results have not been achieved even in the unsteady studies. Meng et al. [23] and Meng et al. [24] indicated that in hovering flight, the average lift force of corrugated wings is 5% lower than that of a flat plate, and corrugations even decrease the aerodynamic forces in forward flight. It has also been argued that flow separation is slightly dependent on wing kinematics. In contrast, the majority of studies on the flapping motion showed that corrugations delayed the separation and produced more lift force [25-29].

In steady experimental studies, different reasons have been proposed to explain the high performance of corrugated surfaces. For instance, Rees et al. [18] have argued that the airflow gets stuck in corrugations valleys and begins to rotate in these valleys gently. Neumann et al. [16] also demonstrated that the aerodynamic performance is related to flow reattachment on the corrugated wing. To be more exact, when the attack angle increases, the flow separates from the leading edge as laminar separation bubbles (LSB). Then the flow again attaches to the corrugated surface. Kessel [14] has measured the pressure on the dragonfly wing and lift and drag forces. Results showed that the negative pressure produced in the valleys of the corrugated surface increases the lift coefficient. In a numerical study, Vargas and Mittal [30] have also confirmed the existence of small vortices in the corrugation valleys. These vortices have also been experimentally observed by Kwok and Mittal [31].

Based on detailed observation, there is a wide range of corrugation patterns, especially along the span-wise direction. The majority of these corrugations with high density could be observed in the vicinity of the wing root. However, with increasing distance from the wing root, the number of corrugations gradually decreases. Therefore, in this study, two cross-sections of a natural dragonfly wing with completely different corrugation patterns are extracted to clarify the role of the wing root and wingtip corrugation patterns on aerodynamic performance. To be more exact, the first cross-section, which is close to the wing root, has more corrugations than the second cross-section, which is close to the wing root. It should be noticed that insect wings generally move at high attack angles (around  $35^\circ$ ) to generate enough lift force for flight [32]. Due to this fact, the performance of cross-sections is also examined compared to a flat plate for a wide range of angles of attacks up to  $30^\circ$ . Also, some empirical studies with more emphasis on the aerodynamic force measurement have been done on the dragonfly wing so far. However, the flow physics around the dragonfly wing has not been thoroughly investigated. Therefore, in the present study, the flow physics of two cross-sections of the dragonfly wing is experimentally examined.

## 2. Experimental set-up

### 3.1 Geometric specifications of dragonfly wing cross-sections

Figure 1 shows the process of fabricating aluminum cross-sections inspired by the dragonfly wing. At first, two cross-sections of the dragonfly wing were cut using a microtome (Figure 1 (a, b)). Then their photos were taken using a microscope with a magnification of 100x and measurement accuracy of 0.001 mm (Figure 1 (c)). During the post-processing, very small corrugations of the cross-sections were neglected (Figure 1(d)). It should be noticed that the first cross-section has corrugations with higher density than the second cross-section. Aluminum plates were chosen to fabricate test cases; therefore, the plates were formed by the aluminum bending machine (Figure 1 (e, f)). Due to the limitation of the Reynolds number, two types of cross-sections are fabricated. The first type of aluminum model with a thickness of 1.5 mm and a chord length of 3 cm is designed for pressure and force measurements. Another kind of aluminum model with a thickness of 5 mm and a chord length of 10 cm is also designed for flow visualization.

### 3.2 Wind tunnel and measurement instruments

The Low Subsonic Wind Tunnel is employed to simulate the flow. This wind tunnel is an open circuit wind tunnel with test section dimensions of  $120 \times 45 \times 45 \text{ cm}^3$  that the maximum velocity in its test section is 20 m/s (Figure 2). Since the Reynolds number insect flight is within a range of  $10 \leq Re \leq 10000$ , the experiments are performed at  $Re = 10000$  and angles of attack between 0 and 30 degrees. In the current study, the PIV technique is also used to measure the velocity field.

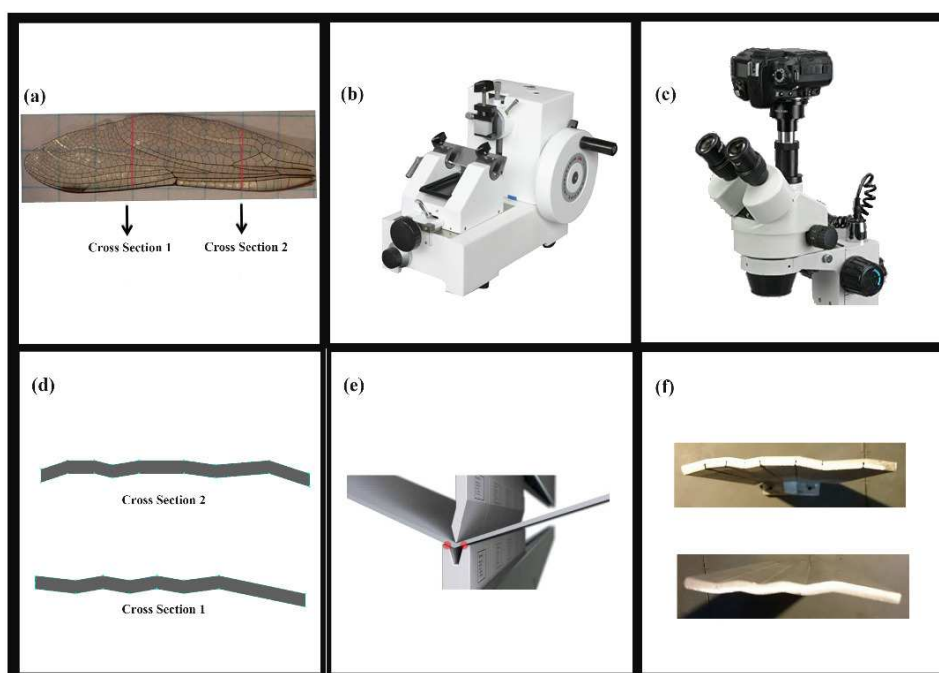


Fig. 1. The process of fabricating two aluminum cross-sections



In this study, the flow velocity is measured by a one-component hotwire anemometer equipped with only 90-10 Platinum-Radium wire with a diameter of 5  $\mu\text{m}$ . Besides, AeroTech smart CTA comprised CTA, and a 24-bit A/D processor is used. Data acquisition is also obtained at a frequency rate of 400 Hz at 10 seconds.

Sensor Technique differential pressure transducers with a maximum capacity of 1kPa and the overall accuracy of 0.1% FS are employed to quantify static pressure. Advantech 4711150 USB-A data acquisition card, which has sixteen 12-bit channels, is established to convert analog data into digital ones. It should be noticed that data is acquired at a frequency of 400 Hz in 10 seconds in all experiments. Test setup and image processing are shown in Figure 3. Also, Figure 4 illustrates the schematic of the pressure hole locations on the cross-section surfaces.

Drag and lift forces are also calculated using the integration of the pressure distribution on the top and bottom of cross-section surfaces. Besides, the force balance is used to evaluate the lift coefficient measurements obtained from the pressure distributions. The force balance comprises a 300-gram L6JI force gauge with an accuracy of 0.2 % FS. In the measurements performed with this system, the data acquisition is performed at 100 Hz for 10 seconds. The measured forces are converted by a 12-bit A/D Advantech 4711150 USB-A module and recorded by a computer.



Fig. 2. The Wind Tunnel of IAUN

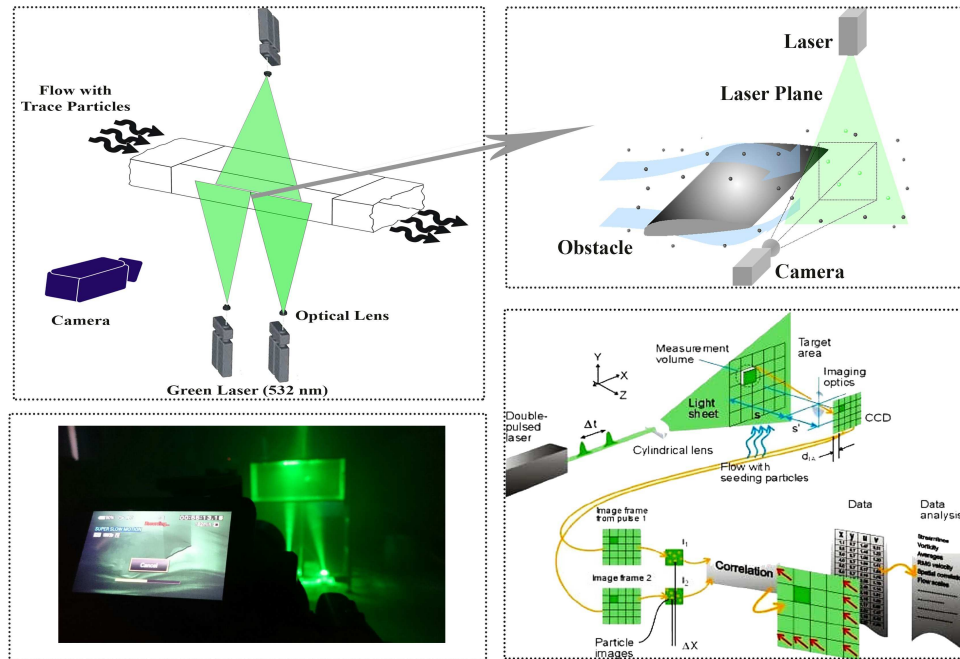
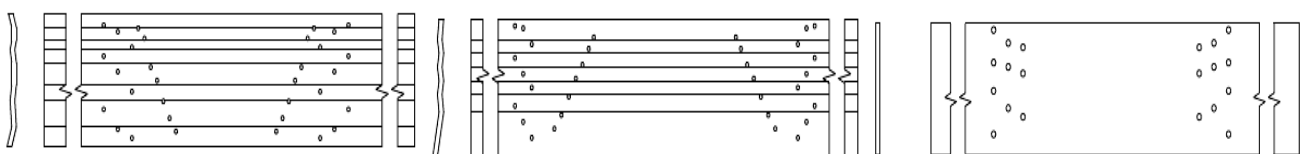


Fig. 3. Test setup and image processing



(a) First cross-section (the vicinity of wing root) (b) Second cross-section (the vicinity of wing tip) (c) Flat plate

Fig. 4. The schematic of pressure hole locations on dragonfly cross-sections and flat plate setup



**Table 1.** This Percentage difference of drag coefficient obtained from different methods with Reference [33].

Re	Geometry	Percentage difference of hotwire results (%)	Percentage difference of PIV technique (%)
688	Circle	4.17	5.84
1377	Circle	4	2
1059	Square	0.8	0.8
2118	Square	2.86	1.43

### 3. Results

#### 4.1 Hotwire anemometer and PIV system validation

To validate the hotwire anemometer and the PIV system, the empirical drag coefficients of circular and square cylinders are compared to references [33] at different Reynolds numbers (Figure 5). Besides, the wake flow behind these geometries are validated against references [34, 35]. Results indicate a satisfactory agreement between the present results and the data as mentioned earlier (Table 1). The wake flow structure behind square and circular cylinders is illustrated in Figure 6.

Figure 7 illustrates the pressure coefficients on the upper surface of the first and second cross-sections at  $Re=10000$ . According to Fig. 7, the behavior of pressure coefficients at different angles of attack is steady. Although slight fluctuations are seen, these fluctuations, are in the range of error band, are negligible. Based on the steady behavior of pressure coefficients, time-averaged pressure distributions were calculated and presented. Besides, the experimental lift coefficients, obtained from pressure distributions and force balance, are compared at  $Re=10000$ . The results of the mentioned comparison are shown in Figure 8. Satisfactory agreements are observed between the results. The lift and drag coefficients of the flat plate obtained from pressure distribution are compared with empirical results in Ref [22] at  $Re=10000$  (Figure 9).

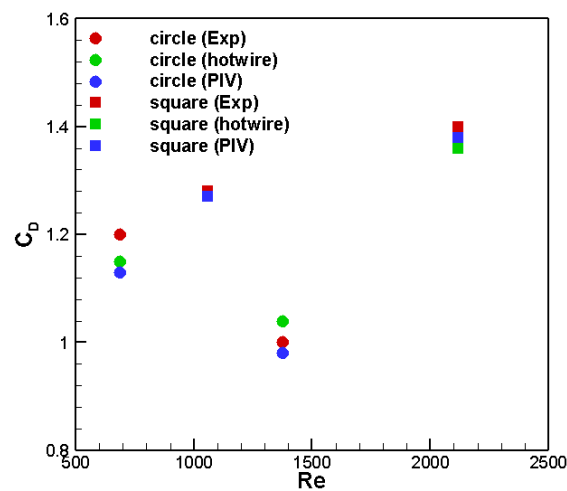


Fig. 5. Drag coefficients obtained from hotwire anemometer and PIV compared to Reference [33]

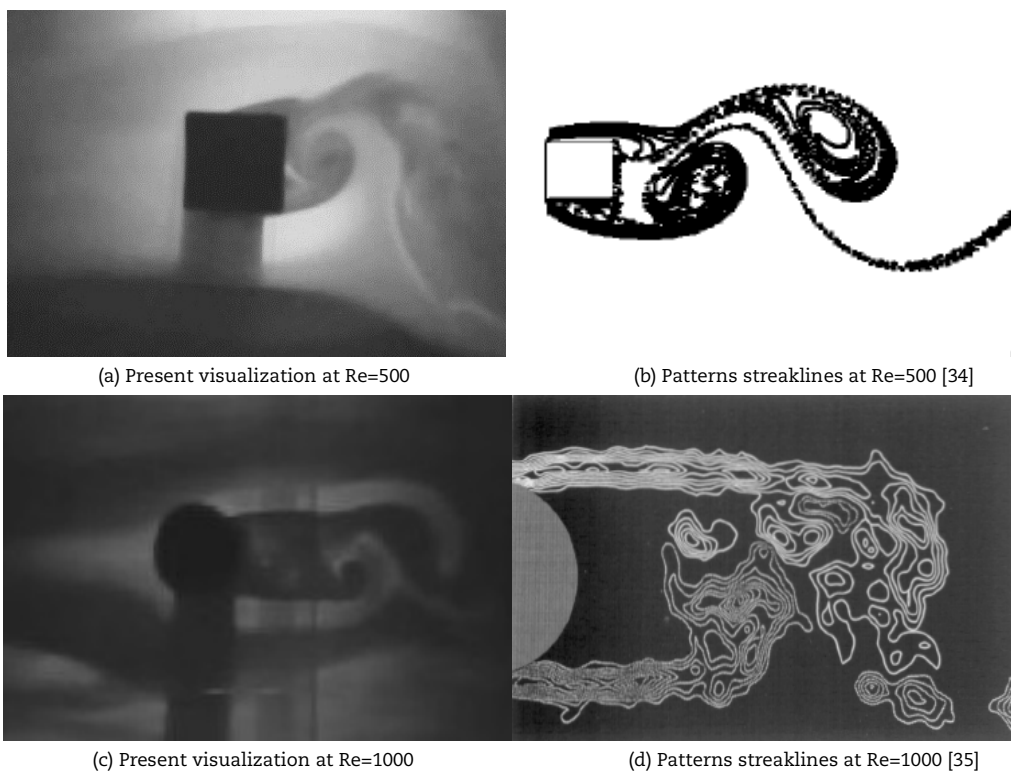
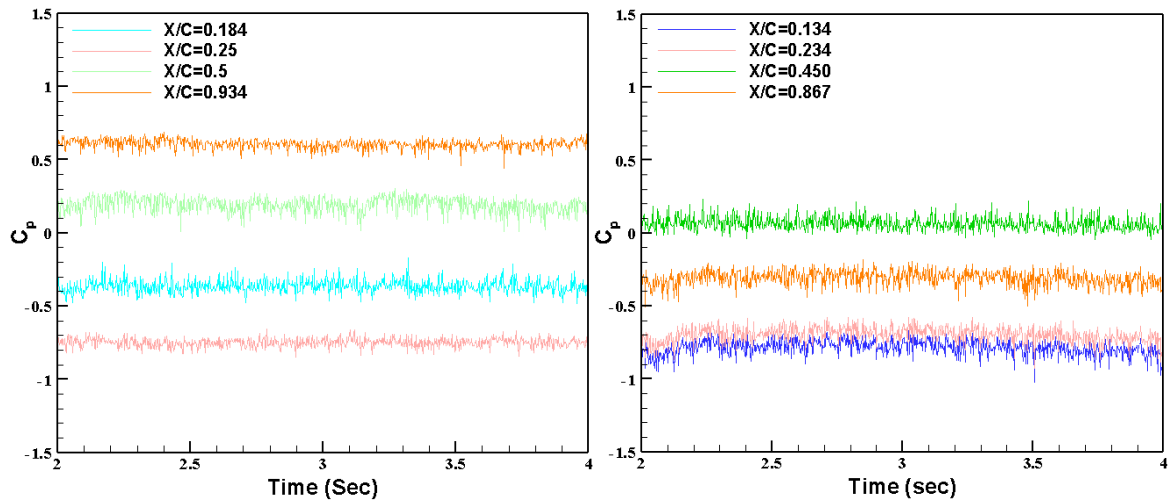
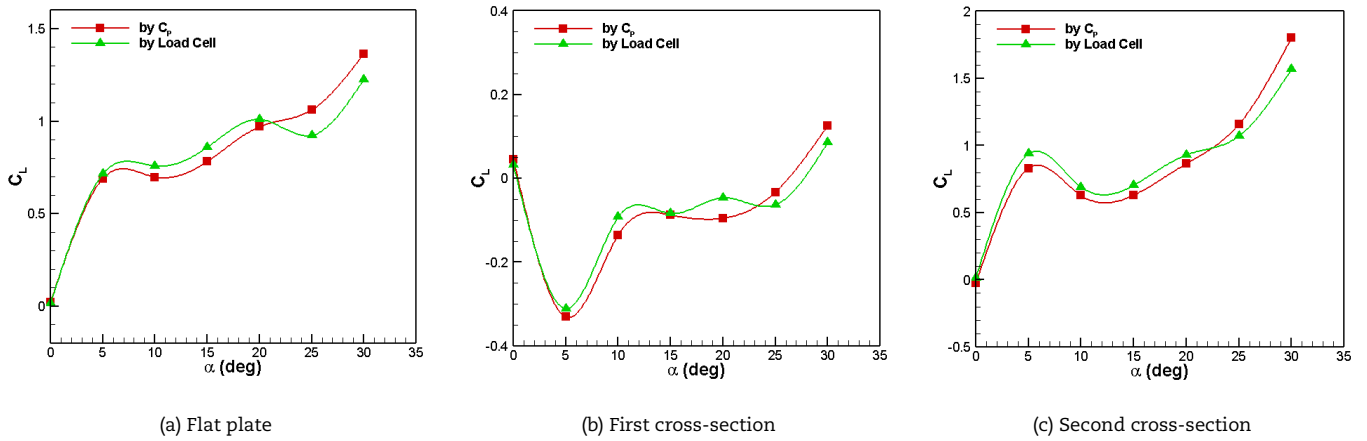


Fig. 6. The wake flow structure behind square and circular cylinders





(a) First cross-section at  $\alpha=5^\circ$  (b) Second cross-section at  $\alpha=15^\circ$   
 Fig. 7. Pressure coefficient on upper surfaces of first and second cross section at  $Re=10000$



(a) Flat plate (b) First cross-section (c) Second cross-section  
 Fig. 8. The Comparison of the Lift Coefficients for different cross-sections at  $Re=10000$

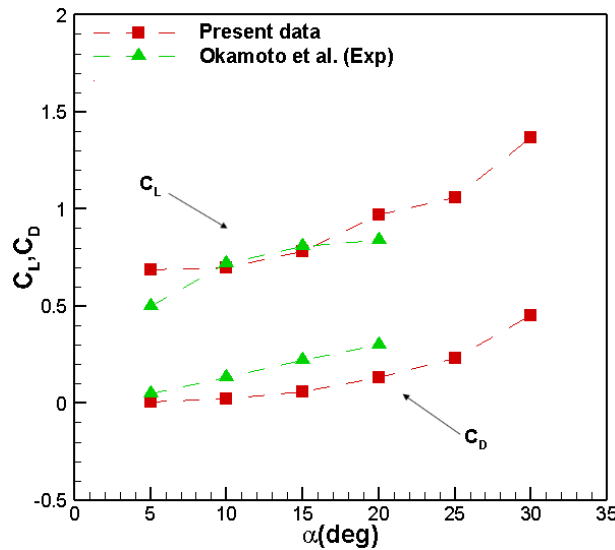


Fig. 9. The aerodynamic coefficients of flat plate at  $Re=10000$

4.2 Analysis of experimental results of cross-sections

In this section, the main focus is on flow physics around cross-sections. At first, a deep insight into the pressure distributions of three cross-sections is given. Then flow physics around sections, and the behavior of aerodynamic coefficients is justified based on pressure distributions.





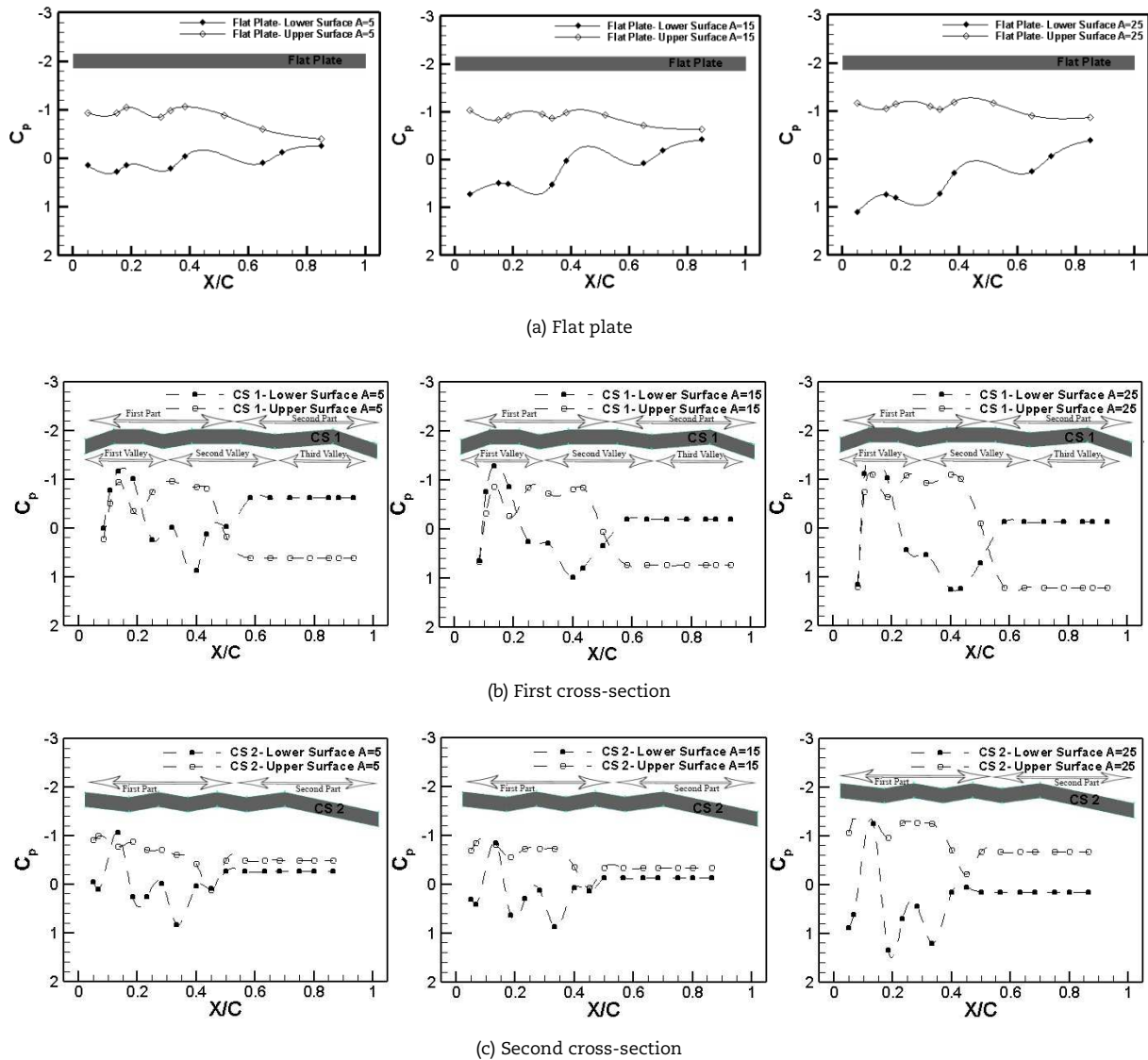


Fig. 10. The Pressure distribution of different cross-sections at  $\alpha = 5^\circ, 15^\circ$  and  $25^\circ$  and  $Re = 10,000$

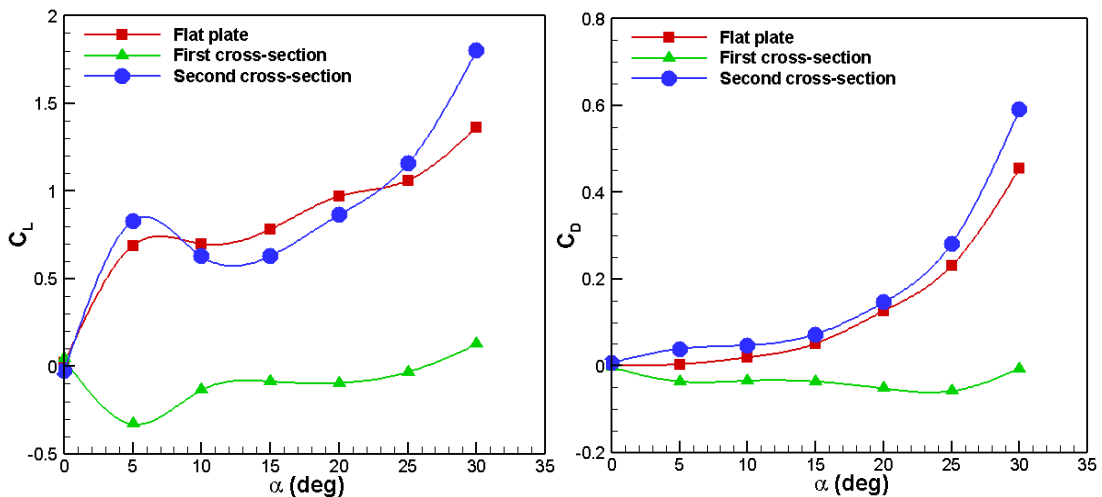


Fig. 11. The Lift and Drag Coefficients of three Cross Sections at  $Re = 10,000$ .

Generally speaking, the surface pressure is usually one order greater than the viscous surface stress; therefore, aerodynamic forces of the wings are mainly generated due to changes in the pressure surface [24, 25]. Figures 10 and 11 show the pressure distributions, and the lift and drag coefficients of the cross-sections at  $Re = 10,000$ , respectively. The difference in the pressure between the upper and lower surfaces of the cross-section generally represents the resultant force.



Based on the pressure distribution of flat plate, at the lower angle of attacks, the lift coefficient of the flat plate dramatically increases; however, the incremental slope of the lift coefficient decreases with increasing angle of attacks. In contrast, an inverse trend in the drag coefficient is observed. With increasing angle of attacks, the drag coefficient slope shows a significant increase. As the angle of attack of the flat plate is increased, the pressure difference between the upper and lower surfaces increases (Figure 10 (a)). To be more exact, for  $\alpha > 15^\circ$ , the difference leads to a dramatic increase in the drag coefficient. Besides, there is a tendency for separation at a higher angle of attack on the upper surface. The separation area on each surface generally leads to a constant pressure distribution on that surface ( $\alpha = 25^\circ$  at  $X/C = 0.8$ , the separation area appears on the suction surface) [36]. Also, two vortices that prevent flow from separating are generated on the upper surface in the vicinity of the leading edge. When the angle of attack increases, pressure reduction is observed on the upper surface near the trailing edge, and pressure increase is seen on the lower surface. With an increase in the angle of attack, pressure reduction is seen on the upper surface near the trailing edge, and no pressure change is seen on the lower surface [37].

According to lift and drag coefficients of the first cross-section, unusual pressure distributions (less pressure on the lower surface compared to the upper surface) on the first cross-section lead to negligible changes in lift and drag coefficients (Figure 11). However, the coefficients achieve slow growth at a higher angle of attack. It should be noticed that pressure drag is negative and close to zero; nevertheless, it seems that total drag will experience positive value with consideration of viscous drag. Flow field around the first and second cross-section is seen in Figure 11. Further investigation of pressure distribution indicates that pressure distribution on the lower surface can be divided into three valleys. Based on this segmentation, the first valley is close to the leading edge, the second valley is located in the middle of cross-section, and the third valley is near to the trailing edge (Figure 10(b)). The substantial decrease in pressure on the first valley shows a strong vortex, leading to accelerating flow. As the angle of attack increases, the suction on the lower surface has become more powerful. On the second valley, pressure distribution reveals the flow separation, but flow reattaches to the lower surface at the end of this valley. The reattachment point indicates the accelerating flow that results in vortex shedding. To be more exact, the clockwise Trailing Edge Vortex (TEV) shows flow velocity on the upper surface is negligible (Figure 12 (b)). Besides, pressure distribution on the upper surface is divided into two parts. A massive reduction in pressure reveals accelerating flow from the leading edge to  $X/C = 0.5$  (first part). Also, from  $X/C = 0.5$  to trailing edge (second part), a clockwise TEV at  $\alpha = 15^\circ$  and  $25^\circ$  clearly shows the flow separation and a significant decrease in flow velocity due to a steep rise in pressure (Figure 12 (b, c)). By increasing the angle of attack, a pressure increase takes place at the trailing edge of the upper and lower surfaces.

Results show that the aerodynamic coefficients of the second cross-section and the flat plate are quite similar (Figure 11). However, at  $\alpha = 5^\circ$ , the lift coefficient of the second cross-section is higher than that of the flat plate. In contrast, at  $\alpha = 15^\circ$ , the lift coefficient of the second cross-section experiences a 24% drop, and the lift coefficient of the flat plate is higher than that of the second cross-section. Due to the pressure distribution on the flat plate, it is evident that the pressure difference between the upper and lower surfaces is increased from  $\alpha = 5^\circ$  to  $15^\circ$ , indicating the increase in resultant force (Figure 10(a)). However, in the second cross-section, the pressure difference between the upper and lower surfaces has a slight reduction (Figure 10(c)). Since the drag coefficient is constant, the reduction of the resultant force is related to the lift coefficient. At  $\alpha = 25^\circ$ , the pressure difference between the upper and lower surfaces of the cross-section dramatically increases, resulting in dramatic increases in lift and drag coefficients. Like the previous segmentation of the first cross-section, the pressure distribution on the upper surface can also be divided into two parts (Figure 10(c)).

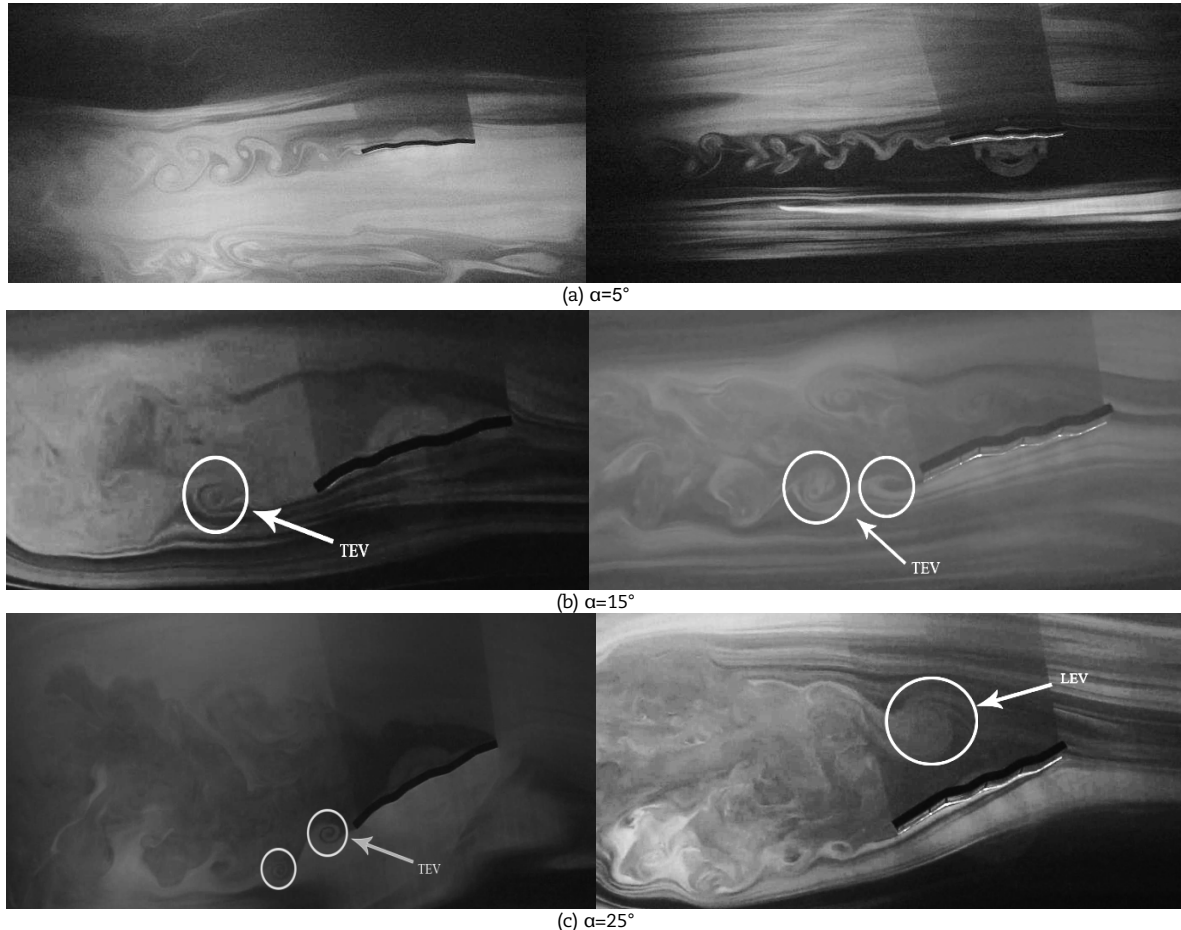


Fig. 12. The Flow Field around the first and second cross-sections at  $Re=10000$



In the first part (from the leading edge to  $x/c=0.5$ ), significant pressure distribution changes have not been seen from  $\alpha = 5^\circ$  to  $15^\circ$ . However, at  $\alpha = 25^\circ$ , a drastic suction occurs in the vicinity of the leading edge. Generally, the flow field investigation around cross-sections can provide a better understanding of aerodynamic force variations. At  $\alpha = 5^\circ$ , flow attaches to the surface due to the low angle of attack, and the geometry of the trailing edge causes the flow to behave periodically in the wake region (Figure 12(a)). Besides, a counter-clockwise Leading-Edge Vortex (LEV) confirms the accelerating flow in the upper surface. Previous investigations showed that corrugations generally increase the negative pressure on the upper surface, which results in the lift force generation; however, this cannot be extended to the lower surface [14]. Due to this fact, local decreases in pressure on the upper surface can be explained. In the entire second part, there is a constant pressure region on the upper surface in all angles of attack. The pressure value of this region at  $\alpha = 15^\circ$  is higher than that of  $\alpha = 5^\circ$ , indicating the flow separation. The existence of a clockwise TEV confirms the separation at  $\alpha = 15^\circ$ . Also, the lower surface comprises three valleys (Figure 10(c)). Some fluctuations in pressure distribution are seen on the lower surface due to the first and second valleys. It seems that the reductions in pressure in these valleys reveal the existence of vortices in these valleys. However, no pressure variations in the third valley indicate flow separation.

Figure 13 shows vorticity layers around the first and second cross-sections at  $Re=10000$ . Previous studies have proved that the creation of vorticity layers in the leading-edge vicinity generally increases the lift coefficient [38]. At  $\alpha = 5^\circ$  and  $15^\circ$ , although vorticity layers are not seen near the leading edge, they exist in the wake region. It seems that vorticity layers downstream have no effects on aerodynamic forces. However, at  $\alpha = 25^\circ$ , vorticity layers are seen on the leading edge of the second cross-section, indicating a significant increase in the lift coefficient (Figure 13(c)).

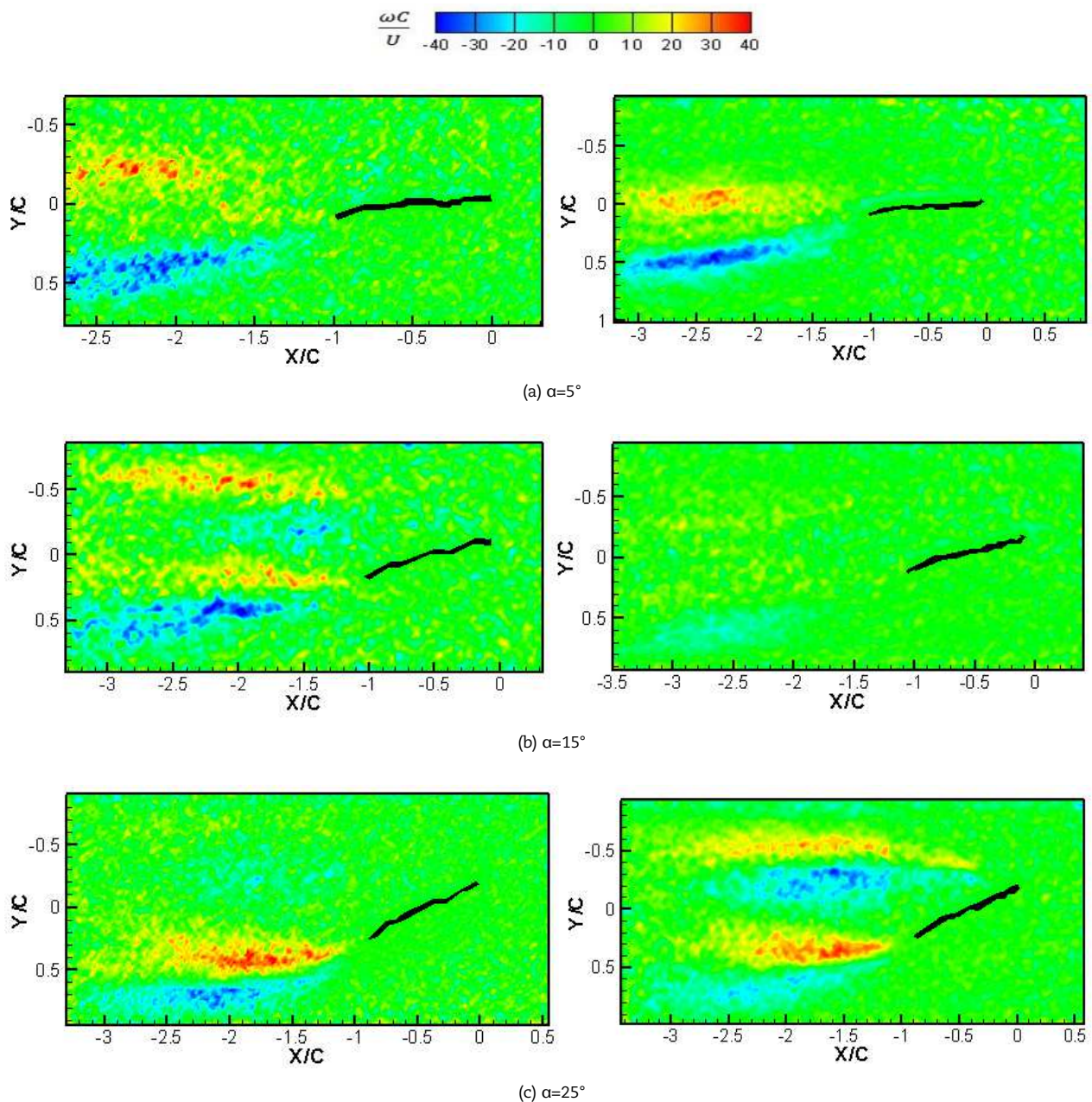


Fig. 13. Time-averaged Vorticity Contours of first and second cross-sections at  $Re=10000$





## 4. Conclusion

An experiment dedicated to the study of the wing root and wingtip corrugation patterns of dragonfly wing at  $Re = 10000$  and angles of attack from  $0^\circ$  to  $30^\circ$  has been performed. For this aim, two cross-sections were extracted from the dragonfly wing. The first cross-section with high-density corrugations was extracted from wing root, whereas the second cross-section with low-density corrugations was extracted from the wingtip. To validate force measurement, a comparison was made between lift coefficients obtained from pressure distributions and force balance. The results are compared at  $Re=10000$ , indicating satisfactory agreements between the results. Therefore, the rest of the aerodynamic forces are calculated based on pressure distributions. Results indicate that less pressure on the lower surface than the upper surface on the first cross-section causes lift and drag coefficients to change negligibly. By increasing the angle of attack, the suction, which is close to the leading edge, has become more powerful on the lower surface. Like the lower surface, suction in pressure takes place near the leading edge on the upper surface at all angles of attack, showing the accelerated flow. Also, the flow separation occurs at  $\alpha > 5^\circ$  due to a clockwise TEV in the second part.

Furthermore, the trend in the aerodynamic coefficients of the second cross-section is similar to the flat plate. However, from  $10^\circ$  to  $20^\circ$ , the lift coefficient of the flat plate is higher than that of the second cross-section. Although the presence of two vortices on the upper surface of the flat plate results in delay in flow separation near the leading edge, a tendency for separation is observed near the trailing edge at  $\alpha = 25^\circ$ . Besides, some fluctuations in pressure distribution on the lower surface of the second cross-section reveal the existence of vorticities on these valleys. However, no pressure variations indicate the flow separation in the third valley. It should be noticed that a dramatic increase in the lift coefficient at  $\alpha = 25^\circ$  is associated with vorticity layers in the leading-edge vicinity of the second cross-section. It seems that all corrugation patterns do not have positive impacts on the aerodynamic forces. The second cross-section can generate adequate aerodynamic forces in comparison to the flat plate and first cross-section. The first cross-section, extracted from wing root, has high-density corrugations; on the contrary, the second cross-section, which is extracted from near the wingtip, has low-density corrugations. According to this fact, it seems that corrugations in the wing root's vicinity have a crucial role in the solidity of insect wings. While the first cross-section generates insufficient lift force, it generates a low drag force. In contrast, corrugations near the wing root play a crucial role in generating enough aerodynamic forces. Due to this fact, a variety of contradictory results has been among previous studies because researchers have not paid attention to corrugated patterns. Therefore, choosing corrugations from the wingtip is essential when generating enough aerodynamic forces is the main priority. Also, when the solidity and low level of drag are essential, corrugation patterns from wing root is the best choice. According the results, force, it generates a low drag force. In contrast, corrugations near the wing root play a crucial role in generating enough aerodynamic forces. Due to this fact, a variety of contradictory results has been among previous studies because researchers have not paid attention to corrugated patterns. According to the results, the second cross-section is a suitable replacement for the flat plate in MAVs because cross-sections extracted from near the wingtip generate higher aerodynamic forces than the flat plate.

## Author Contributions

The research project, inspired by the previous work of R. Lavimi and M. Hojaji, was defined and supervised by M. Hojaji; M.R. Soufivand wholly performed experiments. Besides, authors analyzed the results. R. Lavimi wrote and marshaled the manuscript, but all authors discussed the results, reviewed, and approved the manuscript's final version.

## Acknowledgments

Not applicable.

## Conflict of Interest

The authors declared no potential conflicts of interest with respect to the research, authorship and publication of this article.

## Funding

The authors received no financial support for the research, authorship and publication of this article.

## Data Availability Statements

The datasets generated and/or analyzed during the current study are available from the corresponding author on reasonable request.


## References

- [1] Lee, N., Lee, S., Cho, H., Shin, S., Effect of flexibility on flapping wing characteristics in hover and forward flight, *Computers & Fluids*, 173, 2018, 111-117.
- [2] Shyy, W., Kang, C.K., Chirarattananon, P., Ravi, S., Liu, H., Aerodynamics, sensing and control of insect-scale flapping-wing flight, *Proceedings of the Royal Society A: Mathematical, Physical and Engineering Sciences*, 472(2186), 2016, 20150712.
- [3] Dudley, R., *The Biomechanics of Insect Flight: Form, Function, Evolution*, Princeton University Press, 2000.
- [4] Noda, R., Nakata, T., Liu, H., Effects of wing deformation on aerodynamic performance of a revolving insect wing, *Acta Mechanica Sinica*, 30(6), 2014, 819-827.
- [5] Srygley R.B., Thomas A.L. Unconventional lift-generating mechanisms in free-flying butterflies, *Nature*, 420(6916), 2002, 660-664.
- [6] Taylor G.K., Nudds R.L., Thomas A.L., Flying and swimming animals cruise at a Strouhal number tuned for high power efficiency, *Nature*, 425(6959), 2003, 707-711.
- [7] Lentink D., Flying like a fly, *Nature*, 498(7454), 2013, 306-307.
- [8] Portugal S.J., Hubel T.Y., Fritz J., Heese S., Trobe D., Voelkl B., Hailes S., Wilson A.M., Usherwood J.R., Upwash exploitation and downwash avoidance by flap phasing in ibis formation flight, *Nature*, 505(7483), 2014, 399-402.
- [9] Jafferis N.T., Helbling E.F., Karpelson M., Wood R.J., Untethered flight of an insect-sized flapping-wing microscale aerial vehicle, *Nature*, 570(7762), 2019, 491-495.
- [10] Thomas, A.L., Taylor, G.K., Srygley, R.B., Nudds, R.L., Bomphrey, R.J., Dragonfly flight: free-flight and tethered flow visualizations reveal a diverse array of unsteady lift-generating mechanisms, controlled primarily via angle of attack, *Journal of Experimental Biology*, 207(24), 2004, 4299-4323.
- [11] Soms, C., Luttgies, M., Dragonfly flight: novel uses of unsteady separated flows, *Science*, 228(4705), 1985, 1326-1329.




- [12] Rees, C.J., Aerodynamic properties of an insect wing section and a smooth aerofoil compared, *Nature*, 258(5531), 1975, 141-142.
- [13] Kesel, A.B., Philippi, U., Nachtigall, W., Biomechanical aspects of the insect wing: an analysis using the finite element method, *Computers in Biology and Medicine*, 28(4), 1998, 423-437.
- [14] Kesel, A.B., Aerodynamic characteristics of dragonfly wing sections compared with technical aerofoils, *Journal of Experimental Biology*, 203(20), 2000, 3125-3135.
- [15] McCroskey, W.J., Unsteady airfoils, *Annual Review of Fluid Mechanics*, 114(1), 1982, 285-311.
- [16] Newman, B.G., Savage, S.G., Schouella, D., *Model Tests on a Wing Section of an Aeschna Dragonfly*, Scale Effects in Animal Locomotion, 1977.
- [17] Rudolph, R., Aerodynamic properties of *Libellula quadrimaculata* L. (Anisoptera: Libellulidae), and the flow around smooth and corrugated wing section models during gliding flight, *Odonatologica*, 7(1), 1978, 49-58.
- [18] Rees, C.J., Aerodynamic properties of an insect wing section and a smooth aerofoil compared, *Nature*, 258(5531), 1975, 141-142.
- [19] Okamoto, M., Yasuda, K., Azuma, A., Aerodynamic characteristics of the wings and body of a dragonfly, *Journal of Experimental Biology*, 199(2), 1996, 281-294.
- [20] Wakeling, J.M., Ellington, C.P., Dragonfly flight. I. Gliding flight and steady-state aerodynamic forces, *Journal of Experimental Biology*, 200(3), 1997, 543-556.
- [21] Buckholz, R.H., The functional role of wing corrugations in living systems, *Journal of Experimental Biology*, 108(1), 1986, 93-97.
- [22] Okamoto, M., Azuma, A., Experimental study on aerodynamic characteristics of unsteady wings at low Reynolds number, *AIAA Journal*, 43(12), 2005, 2526-2536.
- [23] Meng, X.G., Xu, L., Sun, M., Aerodynamic effects of corrugation in flapping insect wings in hovering flight, *Journal of Experimental Biology*, 214(3), 2011, 432-444.
- [24] Meng, X., Sun, M., Aerodynamic effects of corrugation in flapping insect wings in forward flight, *Journal of Bionic Engineering*, 8(2), 2011, 140-150.
- [25] Lavimi, R., Hojaji, M., Dehghan Manshadi, M., Investigation of the aerodynamic performance and flow physics on cross sections of Dragonfly wing on flapping and pitching motion in low Reynolds number, *Proceedings of the Institution of Mechanical Engineers, Part G: Journal of Aerospace Engineering*, 233(2), 2019, 589-603.
- [26] Kim, W.K., Ko, J.H., Park, H.C., Byun, D., Effects of corrugation of the dragonfly wing on gliding performance, *Journal of Theoretical Biology*, 260(4), 2009, 523-530.
- [27] Thill, C., Downsborough, J.D., Lai, S.J., Bond, I.P., Jones, D.P., Aerodynamic study of corrugated skins for morphing wing applications, *The Aeronautical Journal*, 114(1154), 2010, 237-244.
- [28] Barnes, C.J., Visbal, M.R., Numerical exploration of the origin of aerodynamic enhancements in [low-Reynolds number] corrugated airfoils, *Physics of Fluids*, 25(11), 2013, 115106.
- [29] Levy, D.E., Seifert, A., Simplified dragonfly airfoil aerodynamics at Reynolds numbers below 8000, *Physics of Fluids*, 21(7), 2009, 071901.
- [30] Vargas, A., Mittal, R., Aerodynamic performance of biological airfoils, In 2nd AIAA Flow Control Conference, Portland, Oregon, 2004.
- [31] Kwok, M., Mittal, R., Experimental investigation of the aerodynamics of a modeled dragonfly wing section, In AIAA region I-MA Student Conference, Charlottesville, Virginia, 2005.
- [32] Cheng, X., Sun, M., Wing-kinematics measurement and aerodynamics in a small insect in hovering flight, *Scientific Reports*, 6, 2016, 25706.
- [33] Pritchard, P.J., Mitchell, J.W., *Fox and McDonald's introduction to fluid mechanics*, John Wiley & Sons, 2016.
- [34] Cheng, M., Whyte, D.S., Lou, J., Numerical simulation of flow around a square cylinder in uniform-shear flow, *Journal of Fluids and Structures*, 23(2), 2007, 207-226.
- [35] Lin, J.C., Towfighi, J., Rockwell, D., Instantaneous structure of the near-wake of a circular cylinder: on the effect of Reynolds, *Journal of Fluids and Structures*, 9(4), 1995, 409-418.
- [36] Amitay, M., Glezer, A., Role of actuation frequency in controlled flow reattachment over a stalled airfoil, *AIAA Journal*, 40(2), 2002, 209-216.
- [37] Tezuka, A., Sunada, Y., Rinoie, K., Surface pressure distributions on 4% circular arc airfoil at low Reynolds number, *Journal of Aircraft*, 45(6), 2008, 2164-2167.
- [38] Hamdani, H.R., Naqvi, A., A study on the mechanism of high-lift generation by an insect wing in unsteady motion at small Reynolds number, *International Journal for Numerical Methods in Fluids*, 67(5), 2011, 581-598.

## ORCID iD

Mohammad Hojaji  <https://orcid.org/0000-0002-6385-7859>

Mohammad Reza Soufivand  <https://orcid.org/0000-0003-2750-4340>

Roham Lavimi  <https://orcid.org/0000-0002-4642-6336>



© 2022 Shahid Chamran University of Ahvaz, Ahvaz, Iran. This article is an open access article distributed under the terms and conditions of the Creative Commons Attribution-NonCommercial 4.0 International (CC BY-NC 4.0 license) (<http://creativecommons.org/licenses/by-nc/4.0/>).

**How to cite this article:** Hojaji M., Soufivand M.R., Lavimi R. An Experimental Comparison between Wing Root and Wingtip Corrugation Patterns of Dragonfly Wing at Ultra-low Reynolds Number and High Angles of Attack, *J. Appl. Comput. Mech.*, 8(4), 2022, 1176-1185. <https://doi.org/10.22055/JACM.2020.33944.2310>

**Publisher's Note** Shahid Chamran University of Ahvaz remains neutral with regard to jurisdictional claims in published maps and institutional affiliations.

